formation and endochondral ossification. Development (Cambridge, England) 137, 901–911.

Herve, M.A., Buteau-Lozano, H., Vassy, R., Bieche, I., Velasco, G., Pla, M., Perret, G., Mourah, S., Perrot-Applanat, M., 2008. Overexpression of vascular endothelial growth factor 189 in breast cancer cells leads to delayed tumor uptake with dilated intratumoral vessels. Am J Pathol 172, 167–178.

Hopf, M., Gohring, W., Kohfeldt, E., Yamada, Y., Timpl, R., 1999. Recombinant domain IV of perlecan binds to nidogens, laminin-nidogen complex, fibronectin, fibulin-2 and heparin. Eur J Biochem 259, 917–925.

Inada, M., Wang, Y., Byrne, M.H., Rahman, M.U., Miyaura, C., Lopez-Otin, C., Krane, S.M., 2004. Critical roles for collagenase-3 (Mmp13) in development of growth plate cartilage and in endochondral ossification. Proc Natl Acad Sci U S A 101, 17192–17197.

Ishijima, M., Rittling, S.R., Yamashita, T., Tsuji, K., Kurosawa, H., Nifuji, A., Denhardt, D.T., Noda, M., 2001. Enhancement of osteoclastic bone resorption and suppression of osteoblastic bone formation in response to reduced mechanical stress do not occur in the absence of osteopontin. J Exp Med 193, 399–404.

Ishijima, M., Tsuji, K., Rittling, S.R., Yamashita, T., Kurosawa, H., Denhardt, D.T., Nifuji, A., Ezura, Y., Noda, M., 2007. Osteopontin is required for mechanical stress-dependent signals to bone marrow cells. J Endocrinol 193, 235–243.

Ivkovic, S., Yoon, B.S., Popoff, S.N., Safadi, F.F., Libuda, D.E., Stephenson, R.C., Daluiski, A., Lyons, K.M., 2003. Connective tissue growth factor coordinates chondrogenesis and angiogenesis during skeletal development. Development (Cambridge, England) 130, 2779–2791.

Jiang, X., Couchman, J.R., 2003. Perlecan and tumor angiogenesis. J Histochem Cytochem 51, 1393–1410.

Karsenty, G., 2003. The complexities of skeletal biology. Nature 423, 316–318.

Kataoka, H., Hamilton, J.R., McKemy, D.D., Camerer, E., Zheng, Y.W., Cheng, A., Griffin, C., Coughlin, S.R., 2003. Protease-activated receptors 1 and 4 mediate thrombin signaling in endothelial cells. Blood 102, 3224–3231.

Klein, G., Conzelmann, S., Beck, S., Timpl, R., Muller, C.A., 1995. Perlecan in human bone marrow: a growth-factor-presenting, but anti-adhesive, extracellular matrix component for hematopoietic cells. Matrix Biol 14, 457–465.

Knox, S.M., Whitelock, J.M., 2006. Perlecan: how does one molecule do so many things? Cell Mol Life Sci 63, 2435–2445.

Knox, S., Merry, C., Stringer, S., Melrose, J., Whitelock, J., 2002. Not all perlecans are created equal: interactions with fibroblast growth factor (FGF) 2 and FGF receptors. J Biol Chem 277, 14657–14665.

Kronenberg, H.M., 2003. Developmental regulation of the growth plate. Nature 423, 332–336.

Kvist, A.J., Johnson, A.E., Morgelin, M., Gustafsson, E., Bengtsson, E., Lindblom, K., Aszodi, A., Fassler, R., Sasaki, T., Timpl, R., Aspberg, A., 2006. Chondroitin sulfate perlecan enhances collagen fibril formation. Implications for perlecan chondrodysplasias. J Biol Chem 281, 33127–33139.

Maes, C., Carmeliet, P., Moermans, K., Stockmans, I., Smets, N., Collen, D., Bouillon, R., Carmeliet, G., 2002. Impaired angiogenesis and endochondral bone formation in mice lacking the vascular endothelial growth factor isoforms VEGF164 and VEGF188. Mech Dev 111, 61–73.

Maes, C., Stockmans, I., Moermans, K., Van Looveren, R., Smets, N., Carmeliet, P., Bouillon, R., Carmeliet, G., 2004. Soluble VEGF isoforms are essential for establishing epiphyseal vascularization and regulating chondrocyte development and survival. J Clin Invest 113, 188–199.

Melrose, J., Smith, S., Whitelock, J., 2004. Perlecan immunolocalizes to perichondrial vessels and canals in human fetal cartilaginous primordia in early vascular and matrix remodeling events associated with diarthrodial joint development. J Histochem Cytochem 52, 1405–1413.

Mongiat, M., Sweeney, S.M., San Antonio, J.D., Fu, J., Iozzo, R.V., 2003. Endorepellin, a novel inhibitor of angiogenesis derived from the C terminus of perlecan. J Biol Chem 278, 4238–4249.

Morita, H., Yoshimura, A., Inui, K., Ideura, T., Watanabe, H., Wang, L., Soininen, R., Tryggvason, K., 2005. Heparan sulfate of perlecan is involved in glomerular filtration. J Am Soc Nephrol 16, 1703–1710.

Nicole, S., Davoine, C.S., Topaloglu, H., Cattolico, L., Barral, D., Beighton, P., Hamida, C.B., Hammouda, H., Cruaud, C., White, P.S., Samson, D., Urtizberea, J.A., Lehmann-Horn, F., Weissenbach, J., Hentati, F., Fontaine, B., 2000. Perlecan, the major proteoglycan of basement membranes, is altered in patients with Schwartz-Jampel syndrome (chondrodystrophic myotonia). Nat Genet 26, 480–483.

Noel, A., Maillard, C., Rocks, N., Jost, M., Chabottaux, V., Sounni, N.E., Maquoi, E., Cataldo, D., Foidart, J.M., 2004. Membrane associated proteases and their inhibitors in tumour angiogenesis. J Clin Pathol 57, 577–584.

Noonan, D.M., Fulle, A., Valente, P., Cai, S., Horigan, E., Sasaki, M., Yamada, Y., Hassell, J.R., 1991. The complete sequence of perlecan, a basement membrane heparan sulfate proteoglycan, reveals extensive similarity with laminin A chain, low density lipoprotein-receptor, and the neural cell adhesion molecule. J Biol Chem 266, 22939–22947.

Olsen, B.R., 1999. Life without perlecan has its problems. J Cell Biol 147, 909–912.

Patel, V.N., Knox, S.M., Likar, K.M., Lathrn, A., Hossain, R., Eftekhari, S., Whitelock, J.M., Elkin, M., Vlodavsky, I., Hoffman, M.P., 2007. Heparanase cleavage of perlecan heparan sulfate modulates FGF10 activity during ex vivo submandibular gland branching morphogenesis. Development (Cambridge, England) 134, 4177–4186.

Rodgers, K.D., Sasaki, T., Aszodi, A., Jacenko, O., 2007. Reduced perlecan in mice results in chondrodysplasia resembling Schwartz-Jampel syndrome. Hum Mol Genet 16, 515–528.

Ruhrberg, C., Gerhardt, H., Golding, M., Watson, R., Ioannidou, S., Fujisawa, H., Betsholtz, C., Shima, D.T., 2002. Spatially restricted patterning cues provided by heparin-binding VEGF-A control blood vessel branching morphogenesis. Genes Dev 16, 2684–2698.

Segev, A., Nili, N., Strauss, B.H., 2004. The role of perlecan in arterial injury and angiogenesis. Cardiovasc Res 63, 603–610.

Smith, S.M., West, L.A., Govindraj, P., Zhang, X., Ornitz, D.M., Hassell, J.R., 2007. Heparan and chondroitin sulfate on growth plate perlecan mediate binding and delivery of FGF-2 to FGF receptors. Matrix Biol 26, 175–184.

Smith, S.M., Shu, C., Melrose, J., 2010. Comparative immunolocalisation of perlecan with collagen II and aggrecan in human foetal, newborn and adult ovine joint tissues demonstrates perlecan as an early developmental chondrogenic marker. Histochem Cell Biol 134, 251–263.

Sottile, J., 2004. Regulation of angiogenesis by extracellular matrix. Biochim Biophys Acta 1654, 13–22.

Staton, C.A., Kumar, I., Reed, M.W., Brown, N.J., 2007. Neuropilins in physiological and pathological angiogenesis. J Pathol 212, 237–248.

Stickens, D., Behonick, D.J., Ortega, N., Heyer, B., Hartenstein, B., Yu, Y., Fosang, A.J., Schorpp-Kistner, M., Angel, P., Werb, Z., 2004. Altered endochondral bone development in matrix metalloproteinase 13-deficient mice. Development (Cambridge, England) 131, 5883–5895.

Takimoto, A., Nishizaki, Y., Hiraki, Y., Shukunami, C., 2009. Differential actions of VEGF-A isoforms on perichondrial angiogenesis during endochondral bone formation. Dev Biol 332, 196–211.

Vu, T.H., Shipley, J.M., Bergers, G., Berger, J.E., Helms, J.A., Hanahan, D., Shapiro, S.D., Senior, R.M., Werb, Z., 1998. MMP-9/gelatinase B is a key regulator of growth plate angiogenesis and apoptosis of hypertrophic chondrocytes. Cell 93, 411–422.

Watanabe, H., Yamada, Y., 2002. Chondrodysplasia of gene knockout mice for aggrecan and link protein. Glycoconj J 19, 269–273.

Watanabe, H., Kimata, K., Line, S., Strong, D., Gao, L.Y., Kozak, C.A., Yamada, Y., 1994. Mouse cartilage matrix deficiency (cmd) caused by a 7 bp deletion in the aggrecan gene. Nat Genet 7, 154–157.

Whitelock, J.M., Murdoch, A.D., Iozzo, R.V., Underwood, P.A., 1996. The degradation of human endothelial cell-derived perlecan and release of bound basic fibroblast growth factor by stromelysin, collagenase, plasmin, and heparanases. J Biol Chem 271, 10079–10086.

Xu, Z., Ichikawa, N., Kosaki, K., Yamada, Y., Sasaki, T., Sakai, L.Y., Kurosawa, H., Hattori, N., Arikawa-Hirasawa, E., 2010. Perlecan deficiency causes muscle hypertrophy, a decrease in myostatin expression, and changes in muscle fiber composition. Matrix Biol 29, 461–470.

Zelzer, E., McLean, W., Ng, Y.S., Fukai, N., Reginato, A.M., Lovejoy, S., D'Amore, P.A., Olsen, B.R., 2002. Skeletal defects in VEGF(120/120) mice reveal multiple roles for VEGF in skeletogenesis. Development (Cambridge, England) 129, 1893–1904.

Zelzer, E., Mamluk, R., Ferrara, N., Johnson, R.S., Schipani, E., Olsen, B.R., 2004. VEGFA is necessary for chondrocyte survival during bone development. Development (Cambridge, England) 131, 2161–2171.

Zhou, Z., Wang, J., Cao, R., Morita, H., Soininen, R., Chan, K.M., Liu, B., Cao, Y., Tryggvason, K., 2004. Impaired angiogenesis, delayed wound healing and retarded tumor growth in perlecan heparan sulfate-deficient mice. Cancer Res 64, 4699–4702.

Zoeller, J.J., Whitelock, J.M., Iozzo, R.V., 2009. Perlecan regulates developmental angiogenesis by modulating the VEGF-VEGFR2 axis. Matrix Biol 28, 284–291.
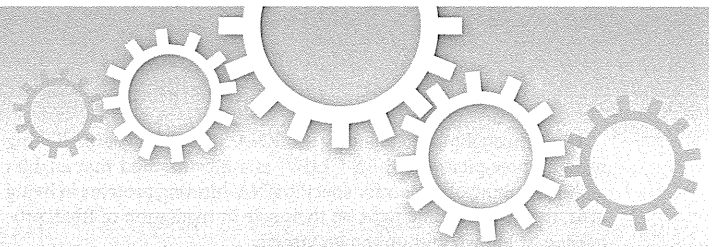
SCIENTIFIC REPORTS

CUGBP1 and MBNL1 preferentially bind to 3' UTRs and facilitate mRNA decay

Akio Masuda[1], Henriette Skovgaard Andersen[2]*, Thomas Koed Doktor[2]*, Takaaki Okamoto[1], Mikako Ito[1], Brage Storstein Andresen[2] & Kinji Ohno[1]

[1]Division of Neurogenetics, Center for Neurological Diseases and Cancer, Nagoya University Graduate School of Medicine, Nagoya, Japan, [2]Department of Biochemistry and Molecular Biology, University of Southern Denmark, Odense M, Denmark.

CUGBP1 and MBNL1 are developmentally regulated RNA-binding proteins that are causally associated with myotonic dystrophy type 1. We globally determined the *in vivo* RNA-binding sites of CUGBP1 and MBNL1. Interestingly, CUGBP1 and MBNL1 are both preferentially bound to 3' UTRs. Analysis of CUGBP1- and MBNL1-bound 3' UTRs demonstrated that both factors mediate accelerated mRNA decay and temporal profiles of expression arrays supported this. Role of CUGBP1 on accelerated mRNA decay has been previously reported, but the similar function of MBNL1 has not been reported to date. It is well established that CUGBP1 and MBNL1 regulate alternative splicing. Screening by exon array and validation by RT-PCR revealed position dependence of CUGBP1- and MBNL1-binding sites on the resulting alternative splicing pattern. This study suggests that regulation of CUGBP1 and MBNL1 is essential for accurate control of destabilization of a broad spectrum of mRNAs as well as of alternative splicing events.

I n recent years, new technologies, such as microarray analysis and high throughput sequencing, have dramatically changed our knowledge on gene expression and revealed that extensive regulation takes place during posttranscriptional RNA processing[1]. Numerous RNA processing elements and regulatory RNA-binding proteins play together in a finely tuned interplay to ensure that different mRNAs are made from the primary transcript from a gene and are present in the right cell at the right time and in the correct amounts. Such complex regulation is of course vulnerable and a rapidly increasing number of human diseases are now known to be caused by misregulated RNA processing[2]. An intriguing example where this kind of disease mechanism is in operation is myotonic dystrophy type 1 (DM1), where aberrant regulation of two RNA-binding proteins, CUG-binding protein 1 (CUGBP1) and muscleblind-like 1 (MBNL1) co-operationally cause some of the disease symptoms. DM1 is the most common form of myotonic dystrophy (DM), and is caused by an expansion of CTG-repeats in the 3' untranslated region (UTR) of the DM protein kinase gene (*DMPK*) on chromosome 19[3–5]. DM1 is a multisystemic disorder and the clinical features include myotonia, muscle degeneration, heart failure, ocular cataracts, impaired glucose tolerance, and mental retardation[6,7]. A dominant negative effect of the *DMPK* mutant allele through RNA gain-of-function has been proposed as the molecular disease mechanism. Many studies support a mechanism where toxic *DMPK* RNA with expanded CUG repeats binds to and sequesters proteins that are important for RNA metabolism including transcription, RNA transport, alternative splicing, translation, and yet unknown processes[6]. The expanded CUG repeats in the *DMPK* mRNA bind to and sequestrate MBNL1 in discrete nuclear foci, which results in depletion of functional MBNL1[8,9]. By a yet unknown mechanism the expanded CUG repeats also activate protein kinase C (PKC), which phosphorylates and stabilizes CUGBP1[10]. Thus, the expanded CUG repeats contribute to DM1 pathogenesis by causing loss of MBNL1 and gain of CUGBP1 activity[11].

Both CUGBP1 and MBNL1 regulate postnatal transitions in alternative splicing patterns during striated muscle development[9,12,13]. Representative targets of CUGBP1 splicing regulation, which are misregulated in DM1 striated muscles, include genes for cardiac troponin T (*TNNT2*)[14,15], insulin receptor (*INSR*)[16], and chloride channel 1 (*CLCN1*)[15,17]. MBNL1 contains four CCCH-type zinc fingers that recognize a YGCY motif that is indeed observed in the CUG repeat (CUGCUG)[18–21]. Mice deficient in *Mbnl1* show aberrant splicing of *Clcn1*, *Tnnt2*, and *Tnnt3*, but not *Insr*[22]. Very recently, MBNL1 was shown to regulate *BIN1* alternative splicing, and dysregulation of *BIN1* splicing in DM1 muscles was suggested to be part of the disease pathology resulting in muscle weakness[23]. Besides an important role in splicing regulation, CUGBP1 mediates mRNA decay of short-lived transcripts by interaction with GU-rich elements in the 3' UTR[24–27]. In addition, CUGBP1 increases the translation of *CDKN1A*[28] and *Mef2a*[29]. In contrast to the multiple functionalities in posttranscriptional gene regulation of CUGBP1, MBNL1 has so far been exclusively recognized as a splicing regulatory *trans*-factor.

High-throughput sequencing of RNA isolated by crosslinking immunoprecipitation (HITS-CLIP)[30] is a new method that enables global mapping of targets for specific RNA-binding proteins in living cells, thereby shedding light on their role in regulation of RNA processing of known and unknown targets.

In the present study, we performed HITS-CLIP analysis for CUGBP1 and MBNL1 on the mouse myoblast cell line C2C12 to extensively characterize their RNA-binding sites and functional roles in RNA processing. We identified position-dependence of CUGBP1/MBNL1-binding sites in regulating exon inclusion or skipping. Interestingly, we discovered that both CUGBP1 and MBNL1 preferentially bind to the 3′ UTR and destabilize target mRNAs. This points to a new important role of MBNL1 and suggests that binding to the 3′ UTRs and destabilization of mRNA are likely to be a fundamental function shared by CUGBP1 and MBNL1.

Results

Genome-wide CUGBP1/MBNL1-RNA interaction maps.
In order to determine global CUGBP1/MBNL1-binding sites *in vivo*, we performed HITS-CLIP experiments using the mouse myoblast cell line, C2C12.

In C2C12 cells, CUGBP1 is constantly expressed throughout myoblast differentiation, whereas expression of MBNL1 is low in undifferentiated cells and gradually increases during differentiation (Supplementary Fig. S1), as previously described[8]. We thus performed HITS-CLIP analysis of CUGBP1 and MBNL1 using undifferentiated and differentiated C2C12 cells, respectively. We also performed CLIP of MBNL1 using undifferentiated cells in three independent experiments, but this yielded an insufficient amount of RNA-protein complexes and failed to yield cDNA libraries suitable for high-throughput sequencing. In the HITS-CLIP analysis of CUGBP1, our first experiment yielded 34,733,815 CLIP tags of 32 nt, of which 29,545,067 (85.06%) were mapped to the mm9 genome allowing at most 2 mismatches and placing reads mapping to multiple locations to a single random site. A second CLIP experiment yielded 10,079,185 CLIP tags of 36 nt, of which 8,516,256 (84.49%) were mapped. In the first MBNL1 CLIP experiment, we obtained 13,218,685 CLIP tags, of which 11,044,152 (83.55%) were mapped, while the second CLIP experiment yielded 13,474,600 CLIP tags with 11,455,886 (85.02%) tags mapped to the mm9 genome. For the analysis of binding motif and binding region annotation, we selected only reads that were aligned uniquely in the genome and removed all potential PCR duplicates by collapsing reads with an identical 5′ start into a single read. This resulted in 177,013 and 130,828 CLIP tags from the two CUGBP1 CLIP experiments, while the two MBNL1 experiments yielded 59,156 and 583,841 CLIP tags respectively.

In an effort to confirm the specificity of our CLIP experiments, we performed CLIP analysis of polypyrimidine tract-binding protein (PTB), a multifunctional RNA-binding protein, using undifferentiated mouse C2C12 cells. We identified 12,841,778 CLIP tags of which 11,184,829 (87.10%) were mapped to the mouse mm9 genome. Removal of non-uniquely aligned reads and PCR duplicates yielded 307,995 unambiguous CLIP tags.

Consensus motifs.
To determine RNA-binding motifs associated with CUGBP1/MBNL1 *in vivo*, we used the motif-finding algorithm, Multiple EM for Motif Elicitation (MEME)[31]. We used SeqMonk to identify likely binding regions, and identified 1,841 CUGBP1-binding regions and 302 MBNL1-binding regions. Comparison of SeqMonk's maximum depth scores between samples indicates that binding regions in each replicated experiment are highly overlapping, while PTB binding regions did not overlap with those of the other four CLIP experiments (Supplementary Fig. S2). The lower number of identified MBNL1 regions supported by two independent experiments (Supplementary Fig. S2b) was likely due to the large difference in the number of CLIP tags in the two

MBNL1 experiments. The regions demonstrate enrichment of GU-rich motifs for CUGBP1 and YGCY-containing motifs for MBNL1 (Fig. 1).

Our *in vivo* binding motifs are in accordance with previously suggested binding motifs for CUGBP1[25,32] and MBNL1[21,33–35]. We identified 1,824 PTB binding regions in the mouse genome and detected a CU-rich motif, which is essentially identical to the motif for PTB recently identified by HITS-CLIP analysis of a human cell line[36].

We also analyzed the CUGBP1 and MBNL1 motifs enriched in regions containing reads with multiple potential mapping locations (Supplementary Fig. S3), and compared them with the motifs with unique mapping (Fig. 1). Following removal of potential PCR duplicates, we observed 699,382 tags that were non-uniquely aligned in the 1st CUGBP1 CLIP experiment, 219,128 tags in the 2nd CUGBP1 CLIP experiment, 105,432 and 216,882 tags in the two MBNL1 CLIP experiments respectively and finally 851,324 tags in the PTB CLIP experiment. We observed that enriched motifs in these regions (Supplementary Fig. S3) are very similar to the CUGBP1 and MBNL1 motifs enriched in the binding regions containing uniquely aligned reads (Fig. 1), suggesting that these regions share the same properties as the uniquely aligned regions and that they may contain functional binding sites.

HITS-CLIP analysis of splicing targets.
We next studied the effects of CUGBP1/MBNL1 binding on alternative splicing. CUGBP1 tags are clustered in intronic regions flanking alternative rather than
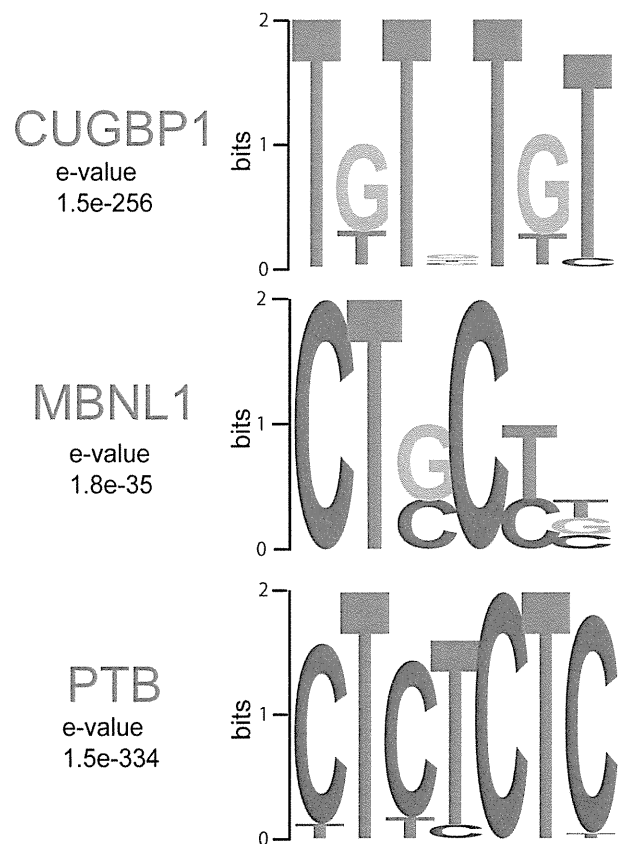

Figure 1 | **Binding motif analysis.** WebLogos of consensus binding motifs of CUGBP1, MBNL1, and PTB generated by the MEME motif analysis tool. The likelihood of finding the indicated motif by chance is indicated as an E-value.

constitutive exons (Fig. 2a). MBNL1 tags are similarly clustered in intronic regions flanking alternative exons, and are also enriched in alternative and constitutive exons. In order to investigate if and how CUGBP1/MBNL1 binding around splice sites regulate alternative splicing, we knocked down these factors by siRNA in undifferentiated C2C12 cells (Supplementary Fig. S4a). We analyzed alterations of splicing globally using the Affymetrix Mouse Exon 1.0 ST Array (GEO accession number, GSE29990) and identified 8 CUGBP1-responsive and 24 MBNL1-responsive exons (Supplementary Table 1, Figs. S5 and S6abc). We also analyzed 29 CUGBP1-tagged and 51 MBNL1-tagged exons/introns known to be alternatively spliced according to the ENSEMBL version e!61, and identified 16 CUGBP1-responsive and 21 MBNL1-responsive exons by RT-PCR (Supplementary Figs. S5 and S6abc). We made the compiled dataset

C, which is comprised of the 24 CUGBP1-regulated exons (15 skipped and 9 included), as well as the compiled dataset M consisting of the 45 MBNL1-regulated exons (25 skipped and 20 included). The datasets include 1 and 9 previously identified target exons of CUGBP1 and MBNL1, respectively (Supplementary Fig. S5). In addition, 9 exons are shared between datasets C and M. Mbnl1 siRNA sufficiently suppressed MBNL1 expression up to day 3 after differentiation (Supplementary Fig. S4b), and we observed that as many as 44 of the 45 MBNL1-regulated exons in dataset M respond similarly to MBNL1 knockdown in both differentiated and undifferentiated cells (Supplementary Figs. S4 and S5).

We also made dataset M2 that includes 26 additional MBNL1-dependent cassette exons (15 skipped and 11 included) that were previously identified in skeletal muscle of MBNL1 knockout mice
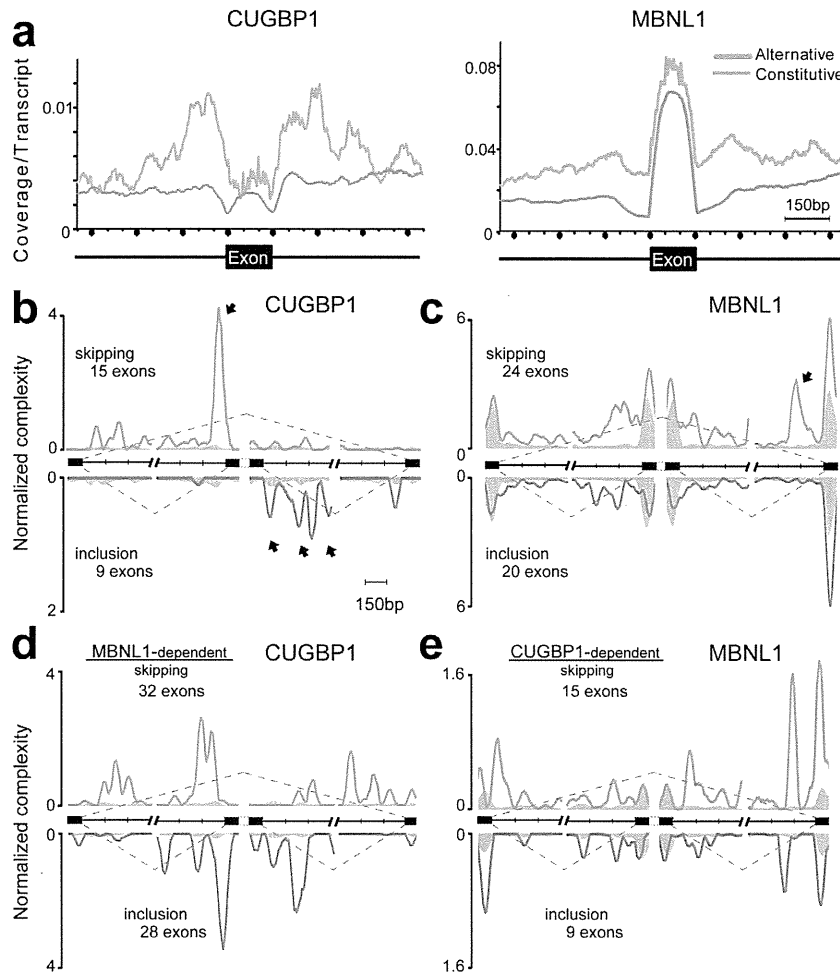

Figure 2 | Mapping of CLIP-tags on exon-intron structures. (a) Distributions of CLIP-tags on constitutively or alternatively spliced exons and the flanking intronic regions. The abscissa indicates an intron-exon-intron structure. The sizes of all the exons are normalized to 150 nucleotides. Numbers of exonic CLIP-tags are also normalized accordingly. Intronic CLIP-tags within 500 nucleotides upstream or downstream of exons are indicated. The number of CLIP-tags is normalized for the number of transcripts belonging to either category of constitutive and alternative exons. (b) Normalized complexity map of CUGBP1 at CUGBP1-dependent splice sites. Twenty-four CUGBP1-regulated splicing events in dataset C in undifferentiated C2C12 cells are compiled. (c) Normalized complexity map of MBNL1 at MBNL1-dependent splice sites. Forty-four MBNL1-regulated splicing events in differentiated C2C12 cells in dataset M are compiled. (d) Normalized complexity map of CUGBP1 at MBNL1-dependent splice sites. Sixty MBNL1-regulated splicing events in undifferentiated C2C12 cells in datasets M and M2 are compiled. (e) Normalized complexity map of MBNL1 at CUGBP1-dependent splice sites. Twenty-four CUGBP1-regulated splicing events in undifferentiated C2C12 cells in dataset C are compiled. Shaded areas represent an average of 100 sets of normalized complexity of 50 (b, c, and d) and 15 (e) randomly selected constitutive exons. Arrows indicate representative peaks that are explained in Results. Graphs represents results of the 2nd CLIP experiments for both CUGBP1 and MBNL1. Resutls of the 1st CLIP experiments are shown in Supplmentary Fig. S7.

(Supplementary Table S2)[33], and found that 18 exons are similarly regulated by *Mbnl1* knockdown in undifferentiated C2C12 cells (Supplementary Fig. S6d and Table S2).

We combined datasets C and M into a single composite pre-mRNA and made integrated RNA maps from our HITS-CLIP reads mapped to the corresponding genomic regions as previously described for Nova[30] and PTB[36]. This showed that CUGBP1 binding to upstream intronic regions facilitates exon skipping, whereas CUGBP1 binding to downstream intronic regions promotes exon inclusion (closed arrows in Fig. 2b and Supplementary Fig. S7a). Results of the 2nd experiments are shown in Fig. 2 and those of the 1st experiments are in Supplementary Fig. S7. In contrast, although the binding sites of MBNL1 are more diffusely distributed and less abundant in regions flanking splice sites (Fig. 2c), MBNL1 binding close to the 3' end of the downstream intron induces exon skipping (closed arrow in Fig. 2c and Supplementary Fig. S7b). The presence of a similar peak in dataset M2 (closed arrow in Supplementary Fig. S7c) further supports this observation.

We next analyzed the interaction between CUGBP1 and MBNL1 in splicing regulation. We made an RNA map of CUGBP1-binding sites in MBNL1-regulated exons from datasets M and M2 (Fig. 2d and Supplementary Fig. S7e), as well as an RNA map of MBNL1-binding sites in CUGBP1-regulated exons from dataset C (Fig. 2e and Supplementary Fig. S7f). Both RNA maps demonstrate the presence of CUGBP1 clusters in MBNL1-responsive exons and vice versa, which suggests that CUGBP1 and MBNL1 are likely to regulate alternative splicing of some of the same exons.

MBNL1 and CUGBP1 both preferentially bind to the 3' UTR. MBNL1 has so far solely been categorized as an exon/intron-binding splicing regulatory protein[6], but to our surprise we found that the majority (55%) of MBNL1-binding regions are located in 3' UTRs (Fig. 3a). The same pattern with preferential binding (53%) in 3' UTRs is observed for CUGBP1, while only 2% of PTB binding regions are located in 3' UTRs (Fig. 3a). Similarly, when HITS-CLIP tags are mapped to the size-normalized positions of all the genes in the mouse genome, CUGBP1 and MBNL1 CLIP tags, but not PTB CLIP-tags, are enriched close to the 3' ends of genes (Fig. 3b). Additionally, 610 3' UTRs, which constitutes 28.7% of the CUGBP1-tagged 3' UTRs and 17.4% of the MBNL1-tagged 3' UTRs, are shared
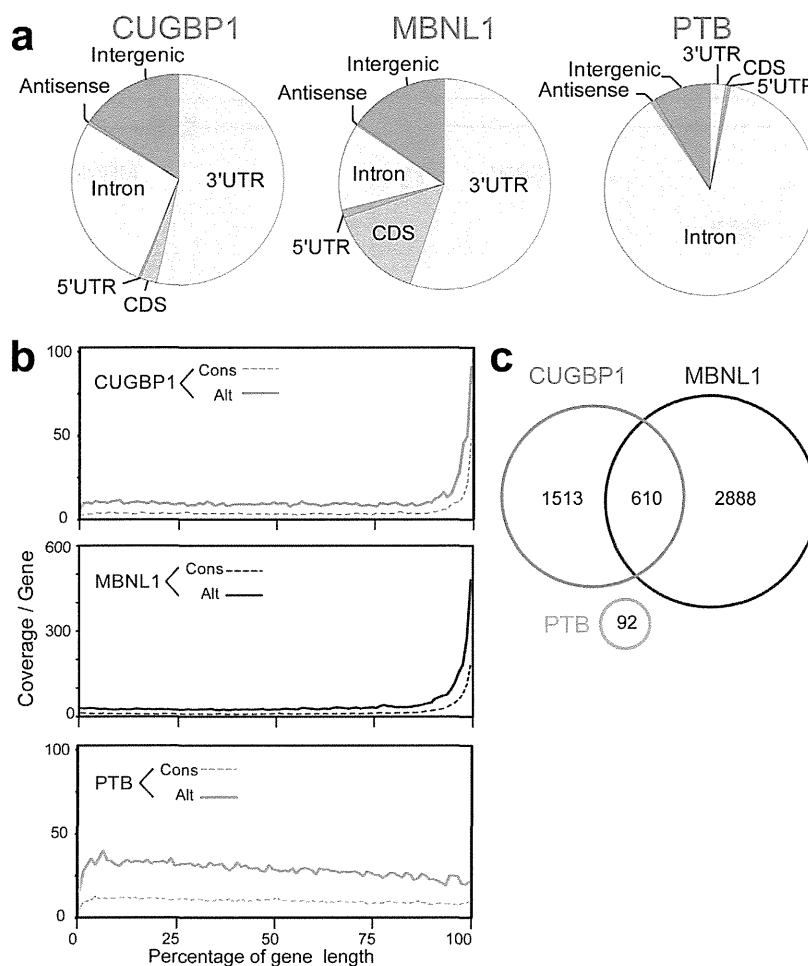

Figure 3 | **Enrichment of CUGBP1 and MBNL1 CLIP-tags in the 3' UTR.** (a) Distributions of CUGBP1, MBNL1, and PTB binding regions. Binding regions are mapped to CDS (coding sequence), 5' and 3' UTRs, introns, intergenic regions (incl. tRNA and rRNA genes), or antisense within genes according to the UCSC knownGene annotation of the NCBI Build 37.1 mouse genome (mm9). Pie-charts show ratios of binding regions mapped to the indicated regions. (b) Distributions of CUGBP1, MBNL1, and PTB CLIP-tags mapped to the relative positions of all the mouse genes. The relative positions of the genes are shown in percentages of the gene length in abscissa. The broken lines represent 15,638 genes with constitutive transcriptional start and end sites (Cons), and the solid lines represent 7,477 genes with alternative transcriptional start or end site (Alt). (c) Venn diagram of the numbers of genes with CUGBP1-, MBNL1-, and PTB-binding regions within the 3' UTR. Binding regions were identified using the SeqMonk software.

between these two proteins (Fig. 3c). All these data document that both CUGBP1 and MBNL1 preferentially bind to 3′ UTRs, indicating that this is a key function of both proteins in RNA processing. This suggests that the functional repertoire of MBNL1 should be expanded and that MBNL1, from being primarily regarded as regulator of alternative splicing, should also be considered as an important regulator of 3′ UTR-mediated processes, such as mRNA stability/degradation.

MBNL1 destabilize mRNAs. To analyze the function of CUGBP1/MBNL1 binding to 3′ UTRs, we made luciferase reporter constructs harboring CUGBP1/MBNL1-binding sites in the 3′ UTR. Since no CLIP tags were observed in the 3′ UTR of *Gapdh* (Supplementary Fig. S8), we made a *luciferase-Gapdh* 3′ UTR expression vector, and then inserted 12 repeats of GT and 7 repeats of CTG immediately after the stop codon of *luciferase* to introduce a CUGBP1-binding site (GU rich motif) and an MBNL1-binding site (YGCY motif), respectively (Fig. 4a). We also inserted 12 AC repeats as a control. Due to the high expression level of CUGBP1 in C2C12 cells we used HEK293 cells for transient transfection of these reporter constructs along with CUGBP1/MBNL1 expression vectors. For the constructs with *Gapdh* 3′ UTR alone or with AC repeats inserted, overexpression of CUGBP1 or MBNL1 had no effect on luciferase activity (Fig. 4b). For the GT repeat construct, overexpression of CUGBP1 decreased the luciferase activity, but MBNL1 had no effect. For the CTG repeat construct overexpression of MBNL1 dramatically decreased the luciferase activity, and also overexpression of CUGBP1 significantly reduced luciferase activity (Fig. 4b). In order to shed light on the mechanism underlying the observed decrease in luciferase activity we investigated the decay of *luciferase* mRNA. The SV40 promoter of the luciferase reporter constructs was replaced with a tet-repressible promoter, and HEK293 Tet-off cells were transiently transfected with these constructs. Doxycycline was added to the medium to stop transcription of the tet-responsive promoter, and the temporal profiles of *luciferase* and *GAPDH* mRNA levels were measured. Overexpression of MBNL1 together with the CTG repeat reporter

construct resulted in highly increased decay of *luciferase* mRNA and CUGBP1 overexpression together with the GT repeat reporter construct also increased mRNA decay. Overexpression of either protein together with the *Gapdh* 3′ UTR control construct did not alter mRNA decay (Fig. 4c). These data demonstrate that binding of CUGBP1 and MBNL1 to the 3′ UTR promotes mRNA decay. To examine whether CUGBP1 and MBNL1 regulate decay of endogenous mRNAs, we next analyzed mRNA stability in actinomycin D treated C2C12 cells by expression arrays following siRNA knock down of CUGBP1 or MBNL1 (GEO accession number, GSE27583). To identify genes with reliable half-life estimates, we restricted our analysis to 195 transcripts using three conditions: (i) half-life between 2.5–5 hrs; (ii) correlation coefficient of fitting to an exponential decay greater than 0.9; and (iii) RMA-normalized signal values more than 100 at all time points. The median half-life of all the transcripts matching these criteria in the control is 3.56 hrs, whereas those from CUGBP1- and MBNL1-knocked down cells are significantly prolonged to 3.91 hrs and 3.73 hrs, respectively (Fig. 5a). We chose four additional representative mRNAs with a cluster of either CUGBP1- or MBNL1-tags in the 3′UTR, and confirmed by real time PCR that knockdown of either CUGBP1 or MBNL1 results in approximately two-fold increase in mRNA half-life of these target mRNAs (Fig. 5b). The half-lives of 100 out of 195 transcripts are prolonged both by knockdown of CUGBP1 and MBNL1, suggesting overlapping activity in the regulation of mRNA decay by CUGBP1 and MBNL1. We next analyzed the relationship between change in mRNA half-life and coverage of HITS-CLIP tags in the 3′ UTRs. We found that genes displaying prolongation of half-lives in response to CUGBP1 knockdown harbors more CUGBP1-tags in their 3′ UTRs, compared to those displaying shortening of half-lives (Fig. 5c). Similarly, genes that display prolongation of their half-lives in response to MBNL1 knockdown have more MBNL1-tags in their 3′ UTRs (Fig. 5c).

Gene Ontology analysis of CUGBP1/MBNL1-bound 3′ UTRs revealed that the terms 'cytoskeletal protein binding, 'transcription factor binding' and 'RNA binding' are significantly overrepresented for CUGBP1- and MBNL1-bound genes (Table 1).
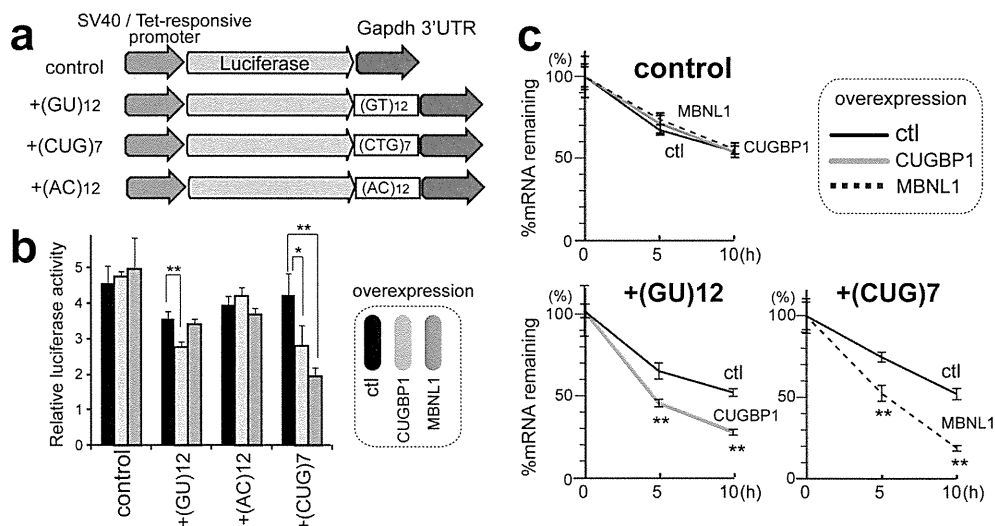

Figure 4 | Decay of *luciferase* mRNA by overexpression of CUGBP1/MBNL1. (a) Schemes of luciferase reporter plasmids harboring *Gapdh* 3′ UTR. Each construct was made carrying either SV40 or tet-responsive promoter. (b) Luciferase activity after overexpression of CUGBP1/MBNL1. HEK293 cells were transfected with the indicated SV40-driven luciferase reporter constructs. Luciferase activity is normalized for the transfection efficiency using co-transfection of pRL/SV40. (c) Decay of luciferase mRNA after overexpression of CUGBP1/MBNL1. HEK293 Tet-off cells were transfected with the indicated tet-responsive promoter-driven luciferase reporter constructs. Doxycycline was added to the medium to stop transcription at time 0. Temporal profiles of luciferase mRNA decay were quantified by real time RT-PCR and are normalized for *Gapdh* mRNA levels. All experiments were triplicated, and the mean and s.d. are indicated (* p < 0.05; ** p < 0.01).
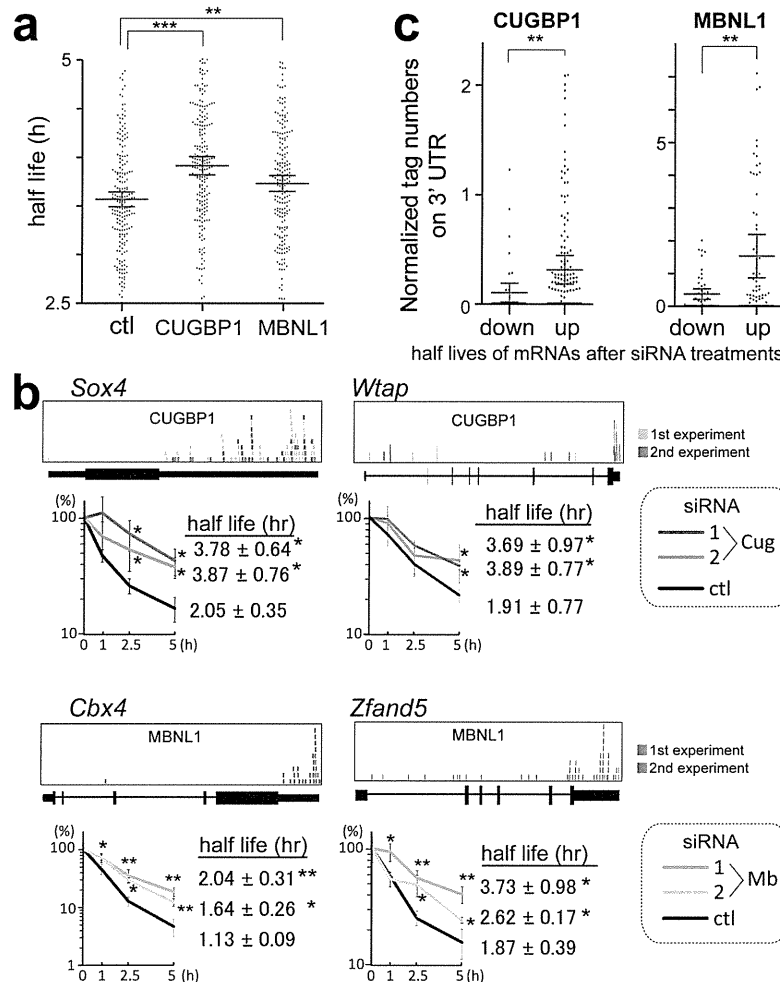
Figure 5 | Global analysis of mRNA decay by expression array of C2C12 cells treated with CUGBP1/MBNL1 siRNA. (a) Half-lives of mRNAs in C2C12 cells with the indicated siRNAs. Red lines represent means and 95% confidence intervals. ** $p < 0.01$ and *** $p < 0.001$. (b) Real-time RT-PCR analysis of the stability of four representative endogenous mRNAs, which were detected by expression arrays. CLIP-tag distributions are shown above each gene structure. C2C12 cells were treated with either control (ctl), CUGBP1 (Cug), or MBNL1 (Mb) siRNA. Actinomycin D was added to the medium to stop transcription at time 0. Temporal profiles of decay of the indicated genes were analyzed by real-time RT-PCR and are normalized for *Gapdh* mRNA levels. All experiments were triplicated, and the mean and s.d. are indicated (* $p < 0.05$ and ** $p < 0.01$). (c) Tag counts in the 3' UTR of each gene are plotted in two categories of prolonging (up) and shortening (down) of half-lives after MBNL1 and CUGBP1 siRNAs. Red lines represent means and 95% confidence intervals. ** $p < 0.01$. Tag counts were normalized by the gene expression level at 0 h of cells treated with control siRNA.

Table 1 | The five most frequent Gene Ontology terms of mRNAs that are bound by CUGBP1 and MBNL1 to the 3' UTR

CLIP data	GO ID	Term	P Value
CUGBP1	GO:0008092	cytoskeletal protein binding	1.58E-06
	GO:0003723	RNA binding	1.40E-04
	GO:0008134	transcription factor binding	9.65E-04
	GO:0051082	unfolded protein binding	0.003184
	GO:0019904	protein domain specific binding	0.006603
MBNL1	GO:0008092	cytoskeletal protein binding	7.31E-20
	GO:0008134	transcription factor binding	2.20E-08
	GO:0003723	RNA binding	0.001893
	GO:0019899	enzyme binding	0.002046
	GO:0032553	ribonucleotide binding	0.004210

We utilized the mRNAs that have more than 8-fold coverage of CLIP tags in their 3'UTR for the analysis by DAVID[53,54].

PITX2 is a homeobox transcription factor that regulates left-right asymmetric morphogenesis[37,38] and it is also deeply implicated in myogenesis during mouse embryonic development[39–41]. We found that the decay of *Pitx2* mRNA is prolonged by knocking down MBNL1, but not CUGBP1 in undifferentiated C2C12 cells (Fig. 6b and c). This is consistent with the fact that *Pitx2* harbors a much higher number of MBNL1-CLIP tags than that of CUGBP1-CLIP tags in the 3′ UTR (Fig. 6a). We also observed that down regulation of both CUGBP1 and MBNL1 decreases the decay of *Myod1* and *Mbnl2* mRNA, but not that of *Gapdh* mRNA (Supplementary

Fig. S8). Similarly, down regulation of CUGBP1 decreases the decay of other myogenic transcription factors such as *Myog* and *Mef2a* mRNAs, and also of *Cugbp2* (Supplementary Fig. S9). Furthermore, knockdown of CUGBP1 and MBNL1 prolongs decay of *Mbnl1* and *Cugbp1* mRNAs, respectively, suggesting a mechanism for cross-regulation of expression of MBNL1, CUGBP1, and their family proteins (Supplementary Fig. S8).

To analyze more directly the role of MBNL1 binding to the 3′ UTR in regulation of mRNA decay, we examined the mRNA stability of firefly luciferase fused with the 3′ UTR of *Pitx2* (Fig. 6a). There are 11 YGCY motifs in the 3′ UTR of *Pitx2*, and 4 of the 11 motifs have MBNL1-CLIP tags. We introduced artificial mutations in these 4 motifs to prevent binding of MBNL1 (Fig. 6a). Consistent with the proposed role for MBNL1 in mRNA decay, we observe that disruption of the MBNL1-binding motifs in the *Pitx2*-3′ UTR abolished responsiveness to MBNL1 knockdown (Fig. 6d). Furthermore, immunoblots demonstrated that MBNL1-knockdown enhanced expression of endogenous PITX2 in C2C12 cells (Fig. 6e). These data suggest that MBNL1 promotes decay of *Pitx2* mRNA and thereby represses expression of the PITX2 protein.

Taken together, all of our data are consistent with a model where CUGBP1 and MBNL1 facilitate mRNA decay through binding to the 3′ UTR of target genes.

Discussion

CUGBP1 and MBNL1 are developmentally regulated RNA-binding proteins that are causally associated with myotonic dystrophy type 1. In this study, we show that both CUGBP1 and MBNL1 preferentially bind to 3′ UTRs and destabilize the bound mRNAs. In particular, we show that CUGBP1 and MBNL1 destabilize myogenic differentiation factors and RNA-binding proteins. In addition, our results confirm and significantly expand the current knowledge of the splicing-regulatory effects of CUGBP1 and MBNL1. Taken together, the data from the present study indicates that CUGBP1 and MBNL1 are closely related and cross regulate alternative splicing and mRNA decay.

MBNL1 binding to 3′ UTRs has not been previously reported. We show for the first time that MBNL1 binds to 3′ UTRs and promotes mRNA decay in both artificial constructs and in endogenous genes. We also demonstrate by expression arrays that both CUGBP1 and MBNL1 facilitate mRNA decay by binding to 3′ UTRs. The present study demonstrates global *in vivo* interactions between CUGBP1 and 3′ UTRs and reveals that CUGBP1 also preferentially binds to 3′ UTR rather than exons/introns. We provide *in vivo* evidence that CUGBP1 facilitates mRNA decay of a broad spectrum of genes in addition to the previously reported genes[25–27,42–44].

Interestingly, we find that MBNL1 promotes decay of *Cugbp1* mRNA and that CUGBP1 promotes decay of *Mbnl1* mRNA, and that this is associated with corresponding changes at the protein level during differentiation of C2C12 cells (Supplementary Fig. S4b). This may suggest that expression of CUGBP1 and MBNL1 are mutually regulated in myogenic differentiation. Kuyumcu-Martinez and colleagues report that expanded CUG repeats of *DMPK* through an unknown mechanism leads to phosphorylation and thereby to stabilization of CUGBP1 in DM1 myoblasts[10]. Our studies additionally suggest that loss of MBNL1 in DM1 could lead to decreased decay of *CUGBP1* mRNA and hence to further increase of CUGBP1 activity. Although CUGBP1 is not upregulated in adult MBNL1-knockout mice, this mechanism could lead to increased misregulation of splicing and decay of the mRNAs of target genes in embryonic development that culminates in the DM1 phenotype.

We find that binding sites for CUGBP1 and MBNL1 are enriched around alternative cassette exons (Fig. 2a). The binding sites for CUGBP1 are prominent in adjacent intronic regions flanking alternative exons. Our functional analysis reveals that binding of CUGBP1 to the upstream intron facilitates exon skipping, whereas
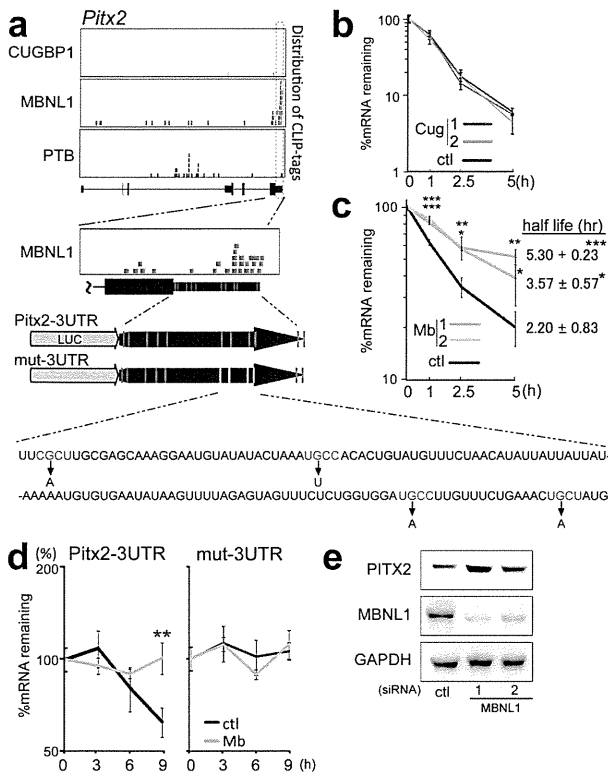

Figure 6 | MBNL1 binds to 3′ UTR of *Pitx2* and facilitates decay of *Pitx2* mRNA. (a) Distributions of MBNL1 CLIP-tags in the *Pitx2*-gene structure, and schemes of luciferase reporter plasmids harboring wild-type (*Pitx2*-3UTR) and mutated (mut-3UTR) 3′ UTRs of *Pitx2*. Red bars indicate locations of native YGCY motifs and yellow bars indicate those of mutated YGCY motifs. Individual mutations disrupting YGCY motifs are shown at the bottom. We introduced U at the 2nd YGCY motif to prevent formation of AU and AC repeats, which constitute a potential binding site of Hu proteins and hnRNP L, respectively. (b and c) Decay of endogenous *Pitx2* mRNA by siRNA-mediated knockdown of CUGBP1 (b) and MBNL1 (c). C2C12 cells were treated with either control (ctl), CUGBP1 (Cug) or MBNL1 (Mb) siRNA. Actinomycin D was added to the medium to stop transcription at time 0. Temporal profiles of decay of the indicated genes were analyzed by real-time RT-PCR and were normalized for *Gapdh* mRNA levels. All experiments were triplicated, and the mean and s.d. are indicated (* p < 0.05; ** p < 0.01; *** p < 0.001). (d) Decay of luciferase mRNA in the Pitx2-3UTR and mut-3UTR constructs after either control (ctl) or MBNL1 (Mb) siRNA in TetON-C2C12 cells. Culture medium was replaced by medium without doxycycline to stop transcription at time 0. Temporal profiles of luciferase mRNA decay are quantified by real-time RT-PCR and are normalized for *Gapdh* mRNA levels. All experiments were triplicated, and the mean and s.d. are indicated (** p < 0.01). (e) Immunoblot of PITX2 in undifferentiated C2C12 cells at 48 hrs after transfection of MBNL1 siRNA.

binding to the downstream intron enhances exon inclusion (Fig. 2b). Interestingly, similar regulation of alternative splicing has been observed for NOVA, FOX2 and PTB[30,45,46], indicating the presence of a common underlying mechanism shared by these proteins.

In contrast to CUGBP1, MBNL1 tags are also enriched in coding exons. Until now, splicing *cis*-elements of MBNL1 have been mapped exclusively to introns, and no exonic *cis*-element has been reported to our knowledge[20,23,34,47,48]. Although MBNL1 preferentially binds to exons, MBNL1 binding to introns is enriched at alternative rather than constitutive splice sites (Fig. 2a. This enrichment is diffusely distributed throughout regions harboring 500 nt upstream or downstream of alternative exons, in contrast to the prominent intronic peaks observed for CUGBP1 tags. This could suggest that MBNL1 needs to bind simultaneously to the target exon and adjacent introns to regulate splicing. Functional analysis of MBNL1 reveals that binding of MBNL1 close to the 3′ end of the downstream intron facilitates exon skipping, whereas no characteristic binding pattern is observed for exons included in response to MBNL1 (Fig. 2c). PTB has also been reported to regulate alternative splicing through binding close to the 3′ end of the downstream intron[36]. In contrast to MBNL1, however, binding of PTB to this region promotes exon inclusion. We similarly find binding of PTB to this region in our HITS-CLIP data in MBNL1-regulated exons (Supplementary Fig. S7d). Interestingly, the MBNL1-binding motif is enriched in PTB-regulated exons[46]. MBNL1 may thus compete for binding with other splicing factors like PTB and regulate alternative splicing events.

Post-transcriptional gene expression regulation is crucial to achieve precise developmental and tissue-specific control of cellular processes. Our studies reveal that CUGBP1 and MBNL1 preferentially bind to the 3′ UTRs of mRNAs encoding RNA-binding proteins and transcription factors, which can regulate cell development. During development of murine skeletal muscles, the nuclear level of MBNL1 increases, while that of CUGBP1 decreases[9,12]. Genes with mRNAs that can be bound both by CUGBP1 and MBNL1 are likely to be down-regulated by CUGBP1 in undifferentiated cells. If these genes need to be tightly down-regulated also in differentiated cells, MBNL1 can substitute for CUGBP1 in order to achieve continued destabilization of the target mRNA. We conclude that finely-tuned expression of CUGBP1 and MBNL1 may be important regulators of myogenic differentiation through precise regulation of both alternative splicing and mRNA stability.

Methods

Antibodies. Antibodies to CUGBP1 (3B1), MHC (H300), myogenin (M225) and PTB (N20) were purchased from Santa Cruz Biotechnology. Anti-GAPDH pAb was purchased from Sigma. Anti-PITX2 pAb was purchased from Abcam. Anti-MBNL1 rabbit serum (A2764) was a kind gift of Dr. Charles A. Thornton at University of Rochester. The specificity of antibodies against CUG BP1 and MBNL1 is supported by the data in previous reports 2,3 and also by our siRNA experiments (Supplementary Fig. S1).

Cell culture. Detailed methods are included in the Supplementary Information.

HITS-CLIP. C2C12 cells were UV-irradiated at 400 mJ and CLIP was performed as previously described[49]. High-throughput 36-bp single-end and 40-bp single-end sequencing was performed using an Illumina Genome Analyzer II. All HITS-CLIP data were registered in ArrayExpress with an accession number E-MTAB-414 and in ENA with an accession number ERP000789. Detailed information is provided in the Supplementary Information.

Bioinformatics analysis. Illumina reads were first prepared by removing the 4-bp tag and filtering sequences composed primarily of Illumina adapter. The resulting reads were mapped to the mouse genome (NCBI Build 37.1/mm9) with default parameters using the BWA[50] mapping software. To extract consensus motifs from the mapped reads, we considered only uniquely aligned reads and first removed duplicate reads to avoid potential PCR-mediated deviations in addition to bias from very highly expressed transcripts. We then extended the reads to 110 nt, the expected mean of the CLIP fragments and used the SeqMonk software (www.bioinformatics.bbsrc.ac.uk/ projects/seqmonk) to identify binding regions by using the program's built-in peak detection algorithm. Peaks were scored using both a reads per peak scoring scheme and a maximum depth scoring scheme (effectively the height of the peak) in order to filter out peaks. For the identification of CUGBP1- and MBNL1-binding regions, we

used PTB as a negative control and removed peaks present in the PTB dataset as well. We then selected CUGBP1 peaks that were present in the two independent CUGBP1 CLIP experiments and MBNL1 peaks that were similarly corroborated by the two MBNL1 experiments. PTB binding regions were identified by removing peaks that were present in either of the four CUGBP1 and MBNL1 experiments. Finally, we restricted the set of binding regions to only those spanning 70–150 bp since this was the fragment length used in the CLIP experiments. We analyzed each dataset using a motif analysis tool, MEME[31], using a background Markov model based on the entire mouse genome.

We analyzed the mapped Illumina reads and binding regions and mapped them to UCSC knownGene annotations[51] of the mouse genome (NCBI Build 37.1/mm9) by writing and running Perl and Excel VBA programs, as well as by running BEDTools utilities[52]. Normalized complexity maps of CUGBP1/MBNL1/PTB-RNA interactions were generated as previously described[30]. For the control, normalized complexity map was similarly generated by analyzing 100 sets of 15 to 50 constitutive exons that were randomly selected from 118,969 constitutive exons in mm9. To identify enriched Gene Ontology terms, we used the Database for Annotation, Visualization and Integrated Discovery (DAVID 6.7)[53,54].

Construction of plasmids. To construct luciferase reporter vectors with the 3′ UTR of *Gapdh* and *Pitx2*, 3′ UTRs of these genes were amplified by PCR. Amplified DNA was ligated into the *Xba*I and *Bam*HI sites of the pGL3-promoter vector (Promega) to substitute for the 3′ UTR of the firefly luciferase gene. DNA fragments harboring GT and CTG repeats were amplified by self-priming PCR using primers terminating in a *Xba*I site, and ligated into the *Xba*I site to make the pGL3P-*Gapdh*-3′ UTR.

To construct tet-responsive luciferase constructs, the tet-responsive promoter region was excised from pTRE-Tight vector (Clontech) with *Xho*I-*Hind*III site and cloned into the *Xho*I-*Hind*III site of the pGL3-promoter vector with the 3′ UTR of *Gapdh* and *Pitx2*. To introduce mutations in 3′ UTR of *Pitx2* in the luciferase construct, we used the QuikChange site-directed mutagenesis kit (Stratagene).

To construct expression vectors for MBNL1 and CUGBP1, the human MBNL1 cDNA and human CUGBP1 cDNA (Open Biosystems) were subcloned into the mammalian bidirectional expression vector pBI-CMV2 (Clontech), which should constitutively expresses the insert and AcGFP1.

RNA interference and transfection. The siRNA duplexes against CUGBP1 and MBNL1 were synthesized by Sigma. The sense sequences of the siRNAs were as follows: Cugbp1-1, 5′-GCUUUGGUUUUGUAAGUUA-3′; Cugbp1-2, 5′-GGCUU-AAAGUGCAGCUCAA-3′; Mbnl1-1, 5′-CACUGGAAGUAUGUAGAGA-3′; and Mbnl1-2, 5′-GCACAAUGAUUGAUACCAA-3′. We purchased the AllStar Negative Control siRNA (1027281) from Qiagen. C2C12 cells were seeded on 24-well plates, and transfected with siRNA using Lipofectamine 2000 (Invitrogen) according to the manufacturer's instructions. Tet-off advanced HEK293 cells were seeded on 96-well plates, and were transfected with luciferase reporter gene constructs using FuGENE 6 (Roche) according to the manufacturer's instructions. At 48 hrs after transfection, cells were either harvested for RNA extraction or processed for isolation of total proteins or nuclear extracts.

RT-PCR for splicing analysis. Total RNA was extracted using Trizol (Invitrogen) according to the manufacturer's instructions. cDNA was synthesized using an oligo-dT primer and ReverTra Ace (Toyobo), and PCR amplifications were performed using GoTaq (Promega) for 30–35 cycles. Sequences of the primers used for PCR are listed in the Supplementary Table S3. The intensities of PCR-amplified spliced products were quantified with the ImageJ 1.42q software (NIH). We then calculated a percentage of exon inclusion (% inclusion) as the ratio of the intensity of the upper band divided by the sum of intensities of all the bands.

Real-time RT-PCR for RNA stability analysis. Total RNA was extracted using RNeasy mini kit (Qiagen) or CellAmp Direct RNA Prep Kit (Takara) according to the manufacturer's instructions. cDNA was synthesized as described above and real-time PCR was performed using the Mx3005P QPCR System (Stratagene) and the SYBR Premix Ex Taq II (Takara). Sequences of the primers used for PCR are listed in Supplementary Table S4.

Microarray analysis. Total RNA was extracted using the RNeasy mini kit according to the manufacturer's instructions. We synthesized and labeled cDNA fragments from 100 ng of total RNA using the GeneChip WT cDNA Synthesis Kit (Ambion). The labeled cDNAs were hybrized to the Affymetrix Mouse Exon 1.0 ST Arrays for splicing analysis or the Affymetrix Mouse Gene 1.0 ST Arrays for analyzing temporal profiles of expression of CUGBP1/MBNL1-targeted genes following the manufacturer's protocols. The robust multichip analysis (RMA) algorithm was used to normalize the array signals across chips with the Affymetrix Expression Console software 1.1.2. All microarray data were uploaded to the Gene Expression Omnibus database (accession numbers, GSE29990 for exon arrays and GSE27583 for expression arrays).

Western blotting. For preparation of total cell lysates, cells were lysed in buffer A (10 mM HEPES pH 7.8, 10 mM KCl, 0.1 mM EDTA, 1 mM DTT, 2 μg/ml Aprotinin, 0.5 mM PMSF, 0.1% NP-40) and incubate on ice for 20 min. After sonication, samples were centrifuged (15,000 rpm, 5 min) and the supernatants were stored at −80°C for further experiments. For preparation of nuclear cell lysates, cells were suspended in 400 μl of buffer A. Nuclei were pelleted, and the cytoplasmic

proteins were carefully removed. The nuclei were then resuspended in buffer C (50 mM HEPES pH 7.8, 420 mM KCl, 0.1 mM EDTA, 5 mM MgCl$_2$, 2% Glycerol, 1 mM DTT, 2 µg/ml Aprotinin, and 0.5 mM PMSF). After vortexing and stirring for 20 min at 4°C, the samples were centrifuged, and the supernatants were stored at −80°C. Samples were analyzed on a 10% SDS polyacrylamide gel, and the proteins were transferred to Immobilon polyvinylidene difluoride membranes (Millipore). Membranes were blocked with 1% BSA in Tris-buffered saline containing 0.05% Tween20 (TBST) for 1 hr, incubated for 1 hr with primary antibodies in TBST, washed three times with TBST, and incubated for 1 hr with horseradish peroxidase-conjugated anti-mouse or -rabbit immunoglobulin (GE) diluted 1 : 5,000 in TBST. After three washes in TBST, the blot was developed with the enhanced chemiluminescence system (GE) according to the manufacturer's instructions.

Luciferase assay. HEK293 cells seeded on a 96 well plate were transfected with 10 ng of pGL3P-*Gapdh*-3′ UTR with or without GT and CTG repeats, 5 ng of pRL/SV40 (Promega), and 40 ng of pBI-CMV2-based CUGBP1 or MBNL1 expression vector using FuGENE 6. At 48 hrs after the transfection, the luciferase activity was measured using the Dual-Luciferase Reporter Assay System (Promega) according to the manufacturer's instructions.

1. Licatalosi, D. D. & Darnell, R. B. RNA processing and its regulation: global insights into biological networks. *Nat Rev Genet* **11**, 75–87 (2010).
2. Wang, G. S. & Cooper, T. A. Splicing in disease: disruption of the splicing code and the decoding machinery. *Nat Rev Genet* **8**, 749–61 (2007).
3. Brook, J. D. et al. Molecular basis of myotonic dystrophy: expansion of a trinucleotide (CTG) repeat at the 3′ end of a transcript encoding a protein kinase family member. *Cell* **68**, 799–808 (1992).
4. Day, J. W. & Ranum, L. P. RNA pathogenesis of the myotonic dystrophies. *Neuromuscul Disord* **15**, 5–16 (2005).
5. Larkin, K. & Fardaei, M. Myotonic dystrophy—a multigene disorder. *Brain Res Bull* **56**, 389–95 (2001).
6. Lee, J. E. & Cooper, T. A. Pathogenic mechanisms of myotonic dystrophy. *Biochem Soc Trans* **37**, 1281–6 (2009).
7. Turner, C. & Hilton-Jones, D. The myotonic dystrophies: diagnosis and management. *J Neurol Neurosurg Psychiatry* **81**, 358–67 (2010).
8. Miller, J. W. et al. Recruitment of human muscleblind proteins to (CUG)(n) expansions associated with myotonic dystrophy. *EMBO J* **19**, 4439–48 (2000).
9. Lin, X. et al. Failure of MBNL1-dependent post-natal splicing transitions in myotonic dystrophy. *Hum Mol Genet* **15**, 2087–97 (2006).
10. Kuyumcu-Martinez, N. M., Wang, G. S. & Cooper, T. A. Increased steady-state levels of CUGBP1 in myotonic dystrophy 1 are due to PKC-mediated hyperphosphorylation. *Mol Cell* **28**, 68–78 (2007).
11. Iwahashi, C. K. et al. Protein composition of the intranuclear inclusions of FXTAS. *Brain* **129**, 256–71 (2006).
12. Kalsotra, A. et al. A postnatal switch of CELF and MBNL proteins reprograms alternative splicing in the developing heart. *Proc Natl Acad Sci U S A* **105**, 20333–8 (2008).
13. Bland, C. S. et al. Global regulation of alternative splicing during myogenic differentiation. *Nucleic Acids Res* (2010).
14. Philips, A. V., Timchenko, L. T. & Cooper, T. A. Disruption of splicing regulated by a CUG-binding protein in myotonic dystrophy. *Science* **280**, 737–41 (1998).
15. Ho, T. H., Bundman, D., Armstrong, D. L. & Cooper, T. A. Transgenic mice expressing CUG-BP1 reproduce splicing mis-regulation observed in myotonic dystrophy. *Hum Mol Genet* **14**, 1539–47 (2005).
16. Savkur, R. S., Philips, A. V. & Cooper, T. A. Aberrant regulation of insulin receptor alternative splicing is associated with insulin resistance in myotonic dystrophy. *Nat Genet* **29**, 40–7 (2001).
17. Charlet, B. N. et al. Loss of the muscle-specific chloride channel in type 1 myotonic dystrophy due to misregulated alternative splicing. *Mol Cell* **10**, 45–53 (2002).
18. Begemann, G. et al. muscleblind, a gene required for photoreceptor differentiation in Drosophila, encodes novel nuclear Cys3His-type zinc-finger-containing proteins. *Development* **124**, 4321–31 (1997).
19. Teplova, M. & Patel, D. J. Structural insights into RNA recognition by the alternative-splicing regulator muscleblind-like MBNL1. *Nat Struct Mol Biol* **15**, 1343–51 (2008).
20. Ho, T. H. et al. Muscleblind proteins regulate alternative splicing. *EMBO J* **23**, 3103–12 (2004).
21. Cass, D. et al. The four Zn fingers of MBNL1 provide a flexible platform for recognition of its RNA binding elements. *BMC Mol Biol* **12**, 20 (2011).
22. Kanadia, R. N. et al. A muscleblind knockout model for myotonic dystrophy. *Science* **302**, 1978–80 (2003).
23. Fugier, C. et al. Misregulated alternative splicing of BIN1 is associated with T tubule alterations and muscle weakness in myotonic dystrophy. *Nature Medicine* **17**, 720–5 (2011).
24. Moraes, K. C., Wilusz, C. J. & Wilusz, J. CUG-BP binds to RNA substrates and recruits PARN deadenylase. *Rna* **12**, 1084–91 (2006).
25. Vlasova, I. A. et al. Conserved GU-rich elements mediate mRNA decay by binding to CUG-binding protein 1. *Mol Cell* **29**, 263–70 (2008).
26. Lee, J. E., Lee, J. Y., Wilusz, J., Tian, B. & Wilusz, C. J. Systematic analysis of cis-elements in unstable mRNAs demonstrates that CUGBP1 is a key regulator of mRNA decay in muscle cells. *PLoS One* **5**, e11201 (2010).
27. Rattenbacher, B. et al. Analysis of CUGBP1 Targets Identifies GU-Repeat Sequences That Mediate Rapid mRNA Decay. *Mol Cell Biol* **30**, 3970–80 (2010).
28. Timchenko, N. A., Iakova, P., Cai, Z. J., Smith, J. R. & Timchenko, L. T. Molecular basis for impaired muscle differentiation in myotonic dystrophy. *Mol Cell Biol* **21**, 6927–38 (2001).
29. Timchenko, N. A. et al. Overexpression of CUG triplet repeat-binding protein, CUGBP1, in mice inhibits myogenesis. *J Biol Chem* **279**, 13129–39 (2004).
30. Licatalosi, D. D. et al. HITS-CLIP yields genome-wide insights into brain alternative RNA processing. *Nature* **456**, 464–9 (2008).
31. Bailey, T. L. & Elkan, C. The value of prior knowledge in discovering motifs with MEME. *Proc Int Conf Intell Syst Mol Biol* **3**, 21–9 (1995).
32. Marquis, J. et al. CUG-BP1/CELF1 requires UGU-rich sequences for high-affinity binding. *Biochem J* **400**, 291–301 (2006).
33. Du, H. et al. Aberrant alternative splicing and extracellular matrix gene expression in mouse models of myotonic dystrophy. *Nat Struct Mol Biol* **17**, 187–93 (2010).
34. Goers, E. S., Purcell, J., Voelker, R. B., Gates, D. P. & Berglund, J. A. MBNL1 binds GC motifs embedded in pyrimidines to regulate alternative splicing. *Nucleic Acids Res* (2010).
35. Kino, Y. et al. Muscleblind protein, MBNL1/EXP, binds specifically to CHHG repeats. *Hum Mol Genet* **13**, 495–507 (2004).
36. Xue, Y. et al. Genome-wide analysis of PTB-RNA interactions reveals a strategy used by the general splicing repressor to modulate exon inclusion or skipping. *Mol Cell* **36**, 996–1006 (2009).
37. Hamada, H., Meno, C., Watanabe, D. & Saijoh, Y. Establishment of vertebrate left-right asymmetry. *Nat Rev Genet* **3**, 103–13 (2002).
38. Yashiro, K., Shiratori, H. & Hamada, H. Haemodynamics determined by a genetic programme govern asymmetric development of the aortic arch. *Nature* **450**, 285–8 (2007).
39. Dong, F. et al. Pitx2 promotes development of splanchnic mesoderm-derived branchiomeric muscle. *Development* **133**, 4891–9 (2006).
40. Shih, H. P., Gross, M. K. & Kioussi, C. Cranial muscle defects of Pitx2 mutants result from specification defects in the first branchial arch. *Proceedings of the National Academy of Sciences of the United States of America* **104**, 5907–12 (2007).
41. Gherzi, R. et al. Akt2-mediated phosphorylation of Pitx2 controls Ccnd1 mRNA decay during muscle cell differentiation. *Cell Death and Differentiation* **17**, 975–83 (2010).
42. Chen, H. H., Xu, J., Safarpour, F. & Stewart, A. F. LMO4 mRNA stability is regulated by extracellular ATP in F11 cells. *Biochem Biophys Res Commun* **357**, 56–61 (2007).
43. Zhang, L., Lee, J. E., Wilusz, J. & Wilusz, C. J. The RNA-binding protein CUGBP1 regulates stability of tumor necrosis factor mRNA in muscle cells: implications for myotonic dystrophy. *J Biol Chem* **283**, 22457–63 (2008).
44. Horb, L. D. & Horb, M. E. BrunoL1 regulates endoderm proliferation through translational enhancement of cyclin A2 mRNA. *Dev Biol* (2010).
45. Yeo, G. W. et al. An RNA code for the FOX2 splicing regulator revealed by mapping RNA-protein interactions in stem cells. *Nat Struct Mol Biol* **16**, 130–7 (2009).
46. Llorian, M. et al. Position-dependent alternative splicing activity revealed by global profiling of alternative splicing events regulated by PTB. *Nat Struct Mol Biol* **17**, 1114–23 (2010).
47. Hino, S. et al. Molecular mechanisms responsible for aberrant splicing of SERCA1 in myotonic dystrophy type 1. *Hum Mol Genet* **16**, 2834–43 (2007).
48. Sen, S. et al. Muscleblind-like 1 (Mbnl1) promotes insulin receptor exon 11 inclusion via binding to a downstream evolutionarily conserved intronic enhancer. *J Biol Chem* **285**, 25426–37 (2010).
49. Ule, J., Jensen, K., Mele, A. & Darnell, R. B. CLIP: a method for identifying protein-RNA interaction sites in living cells. *Methods* **37**, 376–86 (2005).
50. Li, H. & Durbin, R. Fast and accurate long-read alignment with Burrows-Wheeler transform. *Bioinformatics* **26**, 589–95 (2010).
51. Rhead, B. et al. The UCSC Genome Browser database: update 2010. *Nucleic Acids Res* **38**, D613–9 (2010).
52. Quinlan, A. R. & Hall, I. M. BEDTools: a flexible suite of utilities for comparing genomic features. *Bioinformatics* **26**, 841–2 (2010).
53. Huang da, W., Sherman, B. T. & Lempicki, R. A. Systematic and integrative analysis of large gene lists using DAVID bioinformatics resources. *Nat Protoc* **4**, 44–57 (2009).
54. Dennis, G., Jr. et al. DAVID: Database for Annotation, Visualization, and Integrated Discovery. *Genome Biol* **4**, P3 (2003).

Author contributions

A.M., H.S.A, T.O., and M.I. performed the experiments. A.M., T.K.D., B.S.A., and K.O., analyzed the data. A.M., T.K.D., B.S.A. and K.O. prepared the manuscript. All authors reviewed the manuscript.

Additional information

How to cite this article: Masuda, A. *et al.* CUGBP1 and MBNL1 preferentially bind to 3' UTRs and facilitate mRNA decay. *Sci. Rep.* **2**, 209; DOI:10.1038/srep00209 (2012).

班会議プログラム
平成 24 年度・平成 25 年度

厚生労働科学研究費補助金　難治性疾患克服研究事業

希少難治性筋疾患に関する調査研究班
（H24-難治（難）-一般-028）

「　ＩＢＭ分科会　」
H24 年度 班会議プログラム

研究代表者：　　東北大学大学院医学系研究科　神経内科

青木　正志

日　　時　　　平成 25 年 2 月 9 日（土） 14:30〜17:15

会　　場　　　東北大学病院　東病棟 4 階　第 5 会議室

〒980-8574 宮城県仙台市青葉区星陵町 1-2

TEL：022-717-3792（会議室）/ 7453（医局直通）

お願い：演題発表時間 15 分（発表 10 分、討論 5 分）
　　　　発表者はご自身の PC をご持参くださいますようお願いいたします。

開会挨拶　　　　　　　　　　　　　　14：30〜14：35　　　　研究代表者　　　青木　正志

封入体筋炎に関する班員研究発表　　　　14：35〜16：10

Session I　　　　14：35〜15：35　　　　　　　　　　　　　　座　長　　　青木正志

1. 本邦における封入体筋炎の臨床像　：　自験例１８例の検討（14：35〜14：50）

　　　　研究協力者代表：山下　賢
　　　　所　　　　　　属：熊本大学　神経内科
　　　　研 究 協 力 者：○堀　寛子(ほり　ひろこ)1)、山下　賢1)、 本田 省二1)、平原 智雄1)、渡邉 聖
　　　　　　　　　　　　樹1)、山下 太郎1)、前田　寧1)、安東 由喜夫1)
　　　　研究協力者所属：1）熊本大学　神経内科

2. 筋生検にて封入体筋炎が疑われるも、後にＡＬＳと診断された二症例（14：50〜15：05）

　　　　研究協力者代表：樋口　逸郎
　　　　所　　　　　　属：鹿児島大学　神経内科・老年病学
　　　　研 究 協 力 者：○稲森 由恵（いなもり　ゆきえ）1)、樋口 逸郎1)、藤﨑 なつみ1)、橋口 昭大
　　　　　　　　　　　　1)、白石 匡史1)、東　桂子1)、末原 正人1)、髙嶋　博1)
　　　　研究協力者所属：1）鹿児島大学　神経内科・老年病学

3. 封入体筋炎に対するＩＶＩＢ療法の有効性の検討（15：05〜15：20）

　　　　研究協力者代表：○村田 顕也（むらた けんや)
　　　　所　　　　　　属：和歌山県立医科大学　神経内科
　　　　研 究 協 力 者：高　真守1)、宇本 麻衣子1)、伊東 秀文1)
　　　　研究協力者所属：1）和歌山県立医科大学　神経内科

4. 封入体筋炎組織における selenoprotein　N１の免疫組織学的検討（15:20～15:35）

　　　研究協力者代表：日下　博文
　　　所　　　　　属：鹿児島大学大学院　医歯学総合研究科　神経内科　老年病学
　　　研 究 協 力 者：〇中野　智（なかの　さとし)1)、中村 聖香1)、太田 真紀子1)、日下 博文2
　　　　　　　　　　　）、
　　　研究協力者所属：1）大阪市立総合医療センター　神経内科
　　　　　　　　　　　2）関西医科大学　神経内科

　　＊＊＊＊＊＊＊　　　　　コーヒーブレイク　　　　15:35～15:55　　　＊＊＊＊＊＊＊

Session Ⅱ　　　　15:55～17:10　　　　　　　　　　　　　　　座　　　長　　　西野一三

5. 封入体筋炎　update　と希少難治性筋疾患研究班の方向性（15:55～17:10）

　　　研 究 代 表 者：〇青木 正志（あおき　まさし）
　　　所　　　　　属：東北大学大学院医学系研究科　神経内科
　　　研 究 協 力 者：加藤 昌昭1)、堅山 真規1)、割田　仁1)、井泉 瑠美子1)、鈴木 直輝1)、島倉
　　　　　　　　　　　奈緒子1)、安藤 里紗1)、北嶋 康雄1)、高橋 俊明2)、西野 一三3)、森 まど
　　　　　　　　　　　か4)、日下 博文5)、樋口 逸郎6)、村田 顕也7)、山下　賢8)、梶　龍兒9)
　　　研究協力者所属：1）東北大学　神経内科
　　　　　　　　　　　2）国立西多賀病院
　　　　　　　　　　　3）国立精神・神経医療研究センター神経研究所　疾病研究第一部
　　　　　　　　　　　4）国立精神・神経医療研究センター病院　神経内科
　　　　　　　　　　　5）関西医科大学　神経内科
　　　　　　　　　　　6）鹿児島大学医学部・歯学部附属病院　神経内科
　　　　　　　　　　　7）和歌山県立医科大学　神経内科
　　　　　　　　　　　8）熊本大学　神経内科
　　　　　　　　　　　9）徳島大学　神経内科

閉会挨拶　　　　　17:10～17:15　　　　　　　　　　　研究代表者　　　青木　正志

希少難治性筋疾患に関する調査研究班
（H24-難治（難）-一般-028）

「 ＩＢＭ分科会 」
H25 年度 会議プログラム

研究代表者： 東北大学大学院医学系研究科 神経内科学

青木 正志

日　　　時　　平成 26 年 1 月 31 日（金）10:00〜11:55

会　　　場　　都市センターホテル 701 会議室

東京都千代田区平河町 2-4-1

http://www.toshicenter.co.jp/

お願い：演題発表時間 15 分（発表 10 分、討論 5 分）
　　　　発表者はご自身の PC をご持参くださいますようお願いいたします。

研究班事務局：加藤 昌昭、鈴木 直輝、武藤久美子
〒980-8574 宮城県仙台市青葉区星陵町 1-1
東北大学大学院医学系研究科 神経内科学
TEL 022-717-7189 FAX 022-717-7192

開会挨拶　　　　　　　　　　　　10:00〜10:05　　　研究代表者　　青木 正志

封入体筋炎に関する班員研究発表　　　　10:05〜12:30

Session I　　　10:05〜10:50　　　　　　　　　　　　座　長　　青木正志

1. 封入体筋炎に対する経静脈的免疫グロブリン療法の効果（10:05〜10:20）
   研 究 分 担 者：森 まどか
   所　　　　　属：国立精神・神経医療研究センター病院 神経内科
   研 究 協 力 者：〇森まどか1）（もりまどか），西川敦子 1*），山本敏之 1），大矢 寧 1），
   　　　　　　　　　小林 庸子 2），西野一三 3），村田美穂 1）
   研究協力者所属：　1）国立精神・神経医療研究センター病院　神経内科
   　　　　　　　　　2）同病院　リハビリテーション科
   　　　　　　　　　3）同神経研究所　疾病研究第一部
   　　　　　　　　　*現・大阪市立総合医療センター神経内科

2. 封入体筋炎に対する長期継続免疫グロブリン静注(IVIG)療法の有用性（10:20〜10:35）
   研 究 分 担 者：村田　顕也
   所　　　　　属：和歌山県立医科大学 神経内科
   研 究 協 力 者：〇村田顕也 1）（むらたけんや），高　真守 1），阪田麻友美 1），森めぐみ 1），
   　　　　　　　　　中山宜昭 1），檜皮谷泰寛 1），梶本賀義 1），近藤智善 2），伊東秀文 1）
   研究協力者所属：　1）和歌山県立医科大学　神経内科
   　　　　　　　　　2）リハビリテーション花の舎病院

3. IBM の診断における補助検査の有用性（10:35〜10:50）
   研 究 分 担 者：梶　龍兒
   所　　　　　属：徳島大学 神経内科
   研 究 協 力 者：〇松井尚子（まついなおこ），島谷佳光，野寺裕之，和泉唯信，梶 龍兒
   研究協力者所属：　徳島大学神経内科

　　　＊＊＊＊＊＊＊　　　　休憩　　　10:50　〜　11:00　　　＊＊＊＊＊＊＊＊

Session Ⅱ　11：00〜11：45　　　　　　　　　　　　　　　　座　長　　　西野一三

4. 封入体筋炎筋組織における p62/SQSTM1 の発現と nucleophagy （11：00〜11：15）

　　　　研 究 分 担 者：日下　博文

　　　　所　　　　　属：関西医科大学　神経内科

　　　　研 究 協 力 者：○中野　智１）（なかの　さとし），中村聖香１），日下博文２）

　　　　研究協力者所属： 1）大阪市立総合医療センター　神経内科

　　　　　　　　　　　　 2）関西医科大学　神経内科

5. （11：15〜11：30）

　　　　研 究 分 担 者：山下　賢

　　　　所　　　　　属：熊本大学医学部附属病院　神経内科

　　　　研 究 協 力 者：○山下　賢(やました　さとし)1），俵　望1），森　麗1），西田泰斗2），

　　　　　　　　　　　　内野克尚1），永利聡仁3），栗﨑玲一3），中西俊人1），堀 寛子1），

　　　　　　　　　　　　平原智雄1），渡邉聖樹1），上山秀嗣2），山下太郎1），前田 寧1），

　　　　　　　　　　　　安東由喜雄1）

　　　　研究協力者所属： 1）熊本大学医学部附属病院　神経内科

　　　　　　　　　　　　 2）国立病院機構熊本再春荘病院　神経内科

　　　　　　　　　　　　 3）国立病院機構熊本南病院　神経内科

6. （11：30〜11：45）

　　　　研 究 分 担 者：樋口　逸郎

　　　　所　　　　　属：鹿児島大学医学部保健学科理学療法学専攻　基礎理学療法学講座

　　　　研 究 協 力 者：○橋口昭大（はしぐちあきひろ）1），袁　軍輝1），稲森由恵1），白石匡史1），

　　　　　　　　　　　　高嶋　博1），樋口逸郎2）

　　　　研究協力者所属： 1）鹿児島大学大学院医歯学総合研究科　神経内科・老年病学講座

　　　　　　　　　　　　 2）鹿児島大学医学部保健学科理学療法学専攻　基礎理学療法学講座

閉会挨拶　　　　　　　　11：45〜11：50　　　　　　　　　研究代表者　　　青木　正志

厚生労働科学研究費補助金（難治性疾患等克服研究事業(難治性疾患克服研究事業)）

希少難治性筋疾患に関する調査研究班

（H24-難治等（難）-一般-028）

H25 年度 班会議プログラム

研究代表者： 　東北大学大学院医学系研究科　神経内科学

青木　正志

日　　　時　　　平成 26 年 1 月 31 日（金）13:00～16:00

会　　　場　　　都市センターホテル　701 会議室

東京都千代田区平河町 2-4-1

http://www.toshicenter.co.jp/

お願い：演題発表時間 20 分（発表 15 分、討論 5 分）
　　　　発表者はご自身の PC をご持参くださいますようお願いいたします。

研究班事務局：加藤 昌昭、鈴木 直輝、武藤久美子

〒980-8574 宮城県仙台市青葉区星陵町 1-1

東北大学大学院医学系研究科　神経内科学

TEL 022-717-7189　FAX 022-717-7192

開会挨拶　　　　　　　　　　　　　13：00〜13：05　　　研究代表者　　青木　正志

Session I 13：05〜13：45　　　　　　　　　　　　　　座　長　　　西野一三

1. 封入体筋炎　update　と分科会の取り組み（13：05〜13：25）

　　　研 究 代 表 者：○青木　正志（あおき　まさし）
　　　所　　　　　属：東北大学大学院医学系研究科　神経内科学
　　　研 究 協 力 者：加藤　昌昭 1）、竪山　真規 1）、割田　仁 1）、井泉　瑠美子 1）、鈴木　直輝 1）、島倉
　　　　　　　　　　　奈緒子 1）、安藤　里紗 1）、北嶋　康雄 1）、高橋　俊明 2）、西野　一三 3）、森　まど
　　　　　　　　　　　か 4）、日下　博文 5）、樋口　逸郎 6）、村田　顕也 7）、山下　賢 8）、梶　龍兒 9）
　　　研究協力者所属：1）東北大学　神経内科
　　　　　　　　　　　 2）国立西多賀病院
　　　　　　　　　　　 3）国立精神・神経医療研究センター神経研究所　疾病研究第一部
　　　　　　　　　　　 4）国立精神・神経医療研究センター病院　神経内科
　　　　　　　　　　　 5）関西医科大学　神経内科
　　　　　　　　　　　 6）鹿児島大学医学部・歯学部附属病院　神経内科
　　　　　　　　　　　 7）和歌山県立医科大学　神経内科
　　　　　　　　　　　 8）熊本大学　神経内科
　　　　　　　　　　　 9）徳島大学　神経内科

2. 自己貪食空胞性ミオパチー患者の全国実態調査（13：25〜13：45）

　　　研 究 分 担 者：○杉江和馬（すぎえ　かずま）1）2）
　　　所　　　　　属：奈良県立医科大学　神経内科
　　　研 究 協 力 者：西野一三 2）
　　　研究協力者所属：1）奈良県立医科大学　神経内科
　　　　　　　　　　　 2）国立精神・神経医療研究センター　神経研究所　疾病研究第一部

＊＊＊＊＊＊＊　　　休憩　　　13：45　〜　13：55　　　＊＊＊＊＊＊＊

Session II 13：55〜14：55　　　　　　　　　　　　　　座　長　　　林由起子

3. 先天性ミオパチーにおける骨格筋画像データベースの作成（13：55〜14：15）

　　　研 究 分 担 者：小牧　宏文
　　　所　　　　　属：国立精神・神経医療研究センター病院　小児神経科
　　　研 究 協 力 者：○ 石山　昭彦（いしやま　あきひこ）
　　　研究協力者所属：　国立精神・神経医療研究センター病院　小児神経科